Precise half-life determination of the mixed-mirror β-decaying ^{15}O

D. P. Burdette,[1,*] M. Brodeur,[1] D. W. Bardayan,[1] F. D. Becchetti,[2] D. Blankstein,[1] C. Boomershine,[1] L. Caves,[1] S. L. Henderson,[1] J. J. Kolata,[1] B. Liu,[1] J. Long,[1] P. D. O'Malley,[1] and S. Y. Strauss[1]

[1]*Department of Physics, University of Notre Dame, Notre Dame, Indiana 46556 USA*

[2]*Physics Department, University of Michigan, Ann Arbor, Michigan 48109 USA*

(Received 19 December 2019; accepted 6 April 2020; published 14 May 2020)

The half-life of ^{15}O was measured using the β-Counting Station at the University of Notre Dame's Nuclear Science Laboratory. Our new result, $t_{1/2} = 122.308(49)$ s, is the most precise determination to date for ^{15}O, and improves the world average by a factor of 4, yielding $t_{1/2}^{\text{world}} = 122.27(6)$ s. This more precise value will be important for future determinations of V_{ud} using superallowed $T = 1/2$ mirror transitions.

DOI: 10.1103/PhysRevC.101.055504

I. INTRODUCTION

Radioactive decays have been an important process used to determine the nature of forces that influence nuclear matter. The study of nuclear β decay, in particular, has been an effective probe for understanding a wide variety of topics, ranging from the infinitesimal to the astronomical. On the smallest scales, the improvement of experimental techniques, which allow for nuclear observables to be more precisely determined, have provided the most stringent test of the unitarity of the Cabibbo-Kobayashi-Maskawa (CKM) matrix [1]. This constraint was provided by a large experimental effort spanning multiple decades to precisely, and accurately, measure branching ratios, half-lives, and Q_{EC} values for the ensemble of superallowed $0^+ \rightarrow 0^+$ pure Fermi transitions [1].

Although the ensemble of superallowed $0^+ \rightarrow 0^+$ decays currently provides the most precise determination of V_{ud} [2], the accuracy of this result still relies on a few theoretical corrections (δ_R', δ_{NS}^V, δ_C^V, along with a transition independent radiative correction, Δ_R^V) to obtain a reliable value. Recently, the importance of having accurate theoretical corrections was further realized when two new Δ_R^V calculation results [3,4] shifted the extracted V_{ud} value sufficiently enough to create a substantial tension, of up to 3σ, on the unitarity of the CKM matrix [4]. The value of V_{ud} extracted from superallowed $0^+ \rightarrow 0^+$ decays also depends sensitively on the isospin symmetry breaking correction calculation method chosen [5]. As such, it is advantageous to confirm the value of V_{ud} obtained from other superallowed decays. One such decay is superallowed $T = 1/2$ mirror transitions which require the use of the correction δ_C^V [6] also present in pure Fermi decays, and hence could provide a good benchmark for the various calculation methods for δ_C^V. These mixed decays, which have been used to independently extract a value for V_{ud} in the past [7], are more complicated than their $0^+ \rightarrow 0^+$ counterparts since the transition includes Fermi and Gamow-Teller components. Thus, knowledge of the Fermi to Gamow-Teller mixing ratio, ρ, is also required to extract V_{ud}, and accordingly experimental efforts to extract ρ for mirror decays have recently been gaining traction [8–12]. Therefore, it is advantageous to precisely determine all other experimental quantities required to calculate V_{ud}, which are included in the vector part of the corrected ft value, $\mathcal{F}t^{\text{mirror}}$, in anticipation of future determinations of the mixing ratio:

$$\mathcal{F}t^{\text{mirror}} = f_v t(1 + \delta_R')\left(1 + \delta_{NS}^V - \delta_C^V\right). \tag{1}$$

As such, the half-life of the ^{15}O mirror decay has been determined using the β-Counting Station [13] at the Nuclear Science Laboratory (NSL) of the University of Notre Dame.

This mirror decay, in particular, requires a more precise half-life measurement due to inconsistent measurements in the past as presented in Fig. 1. The current world half-life value $t_{1/2}^{\text{world}} = 122.24(23)$ s is derived from the five measurements presented in Table I. Due to the inconsistent nature of this data set, the world value uncertainty includes an inflation factor of 2.6. Hence, it was decided to make a more precise measurement using modern experimental techniques and recalculate the world average.

II. EXPERIMENTAL METHOD

The radioactive beam for this study was created using a stable primary beam of ^{14}N. A NH^- primary beam was generated using a source of negative ions from cesium sputtering (SNICS) with a TiN+TiH cathode, and accelerated to the desired energy using the NSL FN Tandem Van de Graaff accelerator with a terminal voltage of 6.6 MV. This generated about 10 nA of ^{14}N in the 5^+ charge state at the exit of the tandem with an energy of 39 MeV which was selected using the analyzing magnet. The primary beam was then impinged on a deuterium filled gas cell. The gas cell makes use of 4 μm thick Ti windows and a 25 mm long region filled with deuterium gas at about 830 torr. Prior to the measurement, the cell was flushed twice with deuterium gas to minimize contamination.

*dburdett@nd.edu

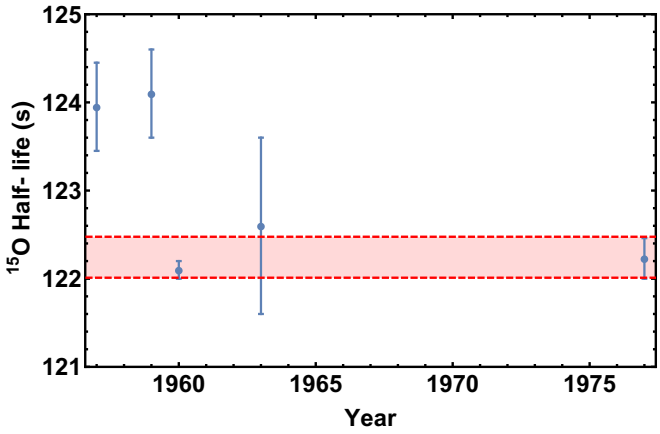

FIG. 1. ^{15}O half-life measurements used in the determination of the world average prior to this work. The red dotted band represents the uncertainty on the world average [6].

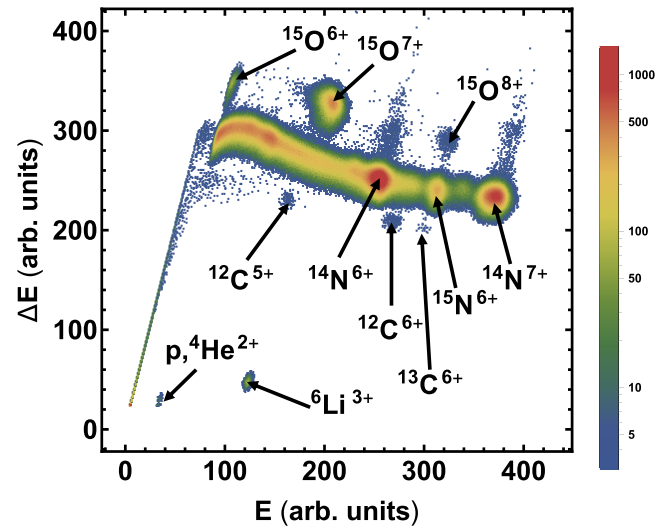

FIG. 2. Particle identification plot, which confirmed the absence of radioactive contaminants, obtained by sending the particle beam through a gas cell.

This created the desired secondary beam, ^{15}O, via a (d, n) transfer reaction in inverse kinematics. The secondary beam was then separated from other reactants and from the primary beam via the two superconducting solenoids of the TwinSol radioactive beam facility [19] coupled with a Faraday cup located at the entrance of the first magnet.

The particle composition of the beam sent to the β-Counting Station for the half-life measurement is shown in Fig. 2. This was obtained by detecting the cocktail beam downstream of the β-Counting Station, with an ionization counter and Si detector telescope. The amounts of energy lost in both the ion counter (ΔE) and in the Si surface barrier detector (E) were measured to determine the various isotopes of the cocktail beam. This process confirmed that no strong radioactive contaminants were present in the beam.

After assessing the composition of the beam and ensuring no radioactive contamination was present, the ionization chamber was removed from behind the β-Counting Station and the paddles were positioned to measure the half-life. The experimental apparatus, shown in Fig. 3, consists of a gold foil mounted on the beam-facing side of a paddle which can be rotated to multiple positions. There were two positions used for this experiment: counting and irradiating. For the irradiation position, the gold is exposed to the radioactive beam for a period of 360 s, or about 3 half-lives. Immediately following irradiation, the foil is rotated into the counting position and the beam is swept away upstream of the accelerator to avoid beam-induced radiation. While in the counting position, β particles resulting from the decay of the radioactive species are counted as a function of time for 3200 seconds, or about 26 half-lives, using a 1 mm thick plastic scintillator coupled to a photomultiplier tube with a light guide. Each run consisted of multiple cycles of both irradiation and counting phases to obtain increased statistics. Typically, runs consisted of

TABLE I. Previous half-life measurements of ^{15}O with precision better than 2.3 s, as this is ten times the uncertainty of the most precise measurement.

Year	Half-life (s)	Ref.
1957	123.95(50)	[14]
1959	124.1(5)	[15]
1960	122.1(1)	[16]
1963	122.6(10)	[17]
1977	122.23(23)	[18]

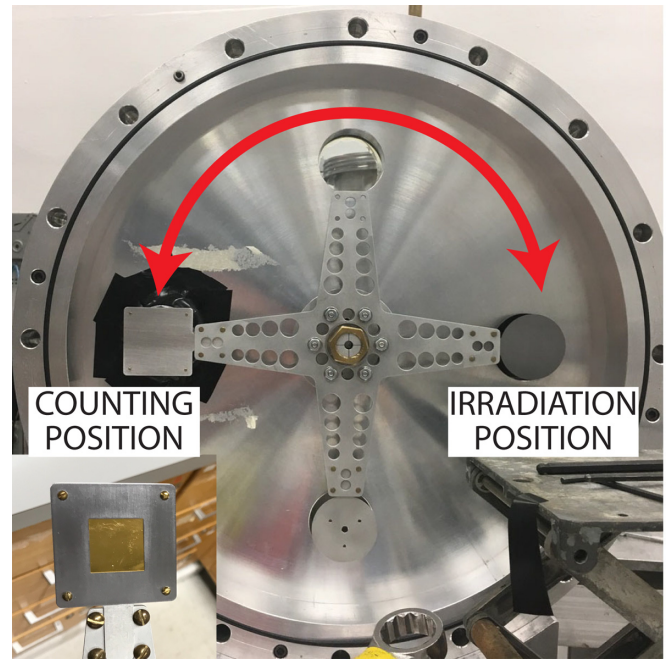

FIG. 3. The β-Counting Station at the NSL. Shown in the bottom left-hand panel is the new gold foil on the tantalum mount. The paddle rotates this foil between counting and irradiation positions as indicated in the figure.

three cycles using identical settings. Runs were carried out at multiple values of photomultiplier tube bias and discriminator threshold voltage to study any systematic trends that may result from these factors. This experimental apparatus has been used in the past for multiple precision half-life measurements, and the reader is directed to those publications for a more detailed description of the setup [13,20–22]. The only modification used for this experiment was a new 0.25 mm thick high-purity (99.999%) gold foil mounted on the paddle held in place by an ultrahigh vacuum cleaned tantalum frame as shown in Fig. 3, which replaced the tantalum foil mounted on an aluminum paddle used in the past. This improvement was aimed at minimizing the production of radioactive contaminants via nuclear reactions on the paddle, through the use of high proton number material.

III. DATA ANALYSIS

Aligning with previous measurements utilizing the β-Counting Station, the data were analyzed with a long-established fitting routine provided by [23]. This procedure allows for the correction of dead-time losses in data acquisition that are inherent to any counting experiment and minimizes the bias in the obtained half-life from the fitting procedure. A conservative dead time used for the analysis was explicitly determined for this measurement as 56.22(14) μs, as outlined in Sec. III D 1.

After determining the dead time, the data were screened on a cycle-by-cycle basis to ensure a consistent data set. All fits first assumed a contaminant-free decay rate equation:

$$r(t) = r_0 \exp[-\ln(2)t/t_{1/2}] + b, \tag{2}$$

with the fit parameter minimization routine described in [23]. Each cycle was first fitted individually, and it was concluded that there were no incomplete cycles (Sec III A). Then, the sum of individual cycles taken with identical systematic settings were fit to determine if any combination of settings had an effect on the measured half-life (Sec. III B). The high statistics result was then obtained from a sum fit of the data where all cycles were summed together (Sec. III C). Finally, multiple sources of systematic uncertainty were taken into account to determine the estimated uncertainty of this measurement (Sec. III D).

A. Cycle-by-cycle analysis

A total of 44 different cycles were taken to obtain enough data to get a high statistics result. Most of the cycles lasted 3200 seconds, or 26 half-lives of ^{15}O, to obtain a good measurement of the background and ensure that there was minimal ^{15}O remaining on the foil from cycle to cycle. Furthermore, 8 of the 44 cycles were twice as long, and taken throughout the experiment with the purpose of searching for long-lived contaminants impacting the measurement. Various combinations of systematic settings were used for the cycles to probe any influence different settings might have on the measured half-life. The initial check of their influence is to determine the half-life independently with data from each cycle and ensure the results are statistically consistent. The resulting half-life for each cycle is shown in Fig. 4. The weighted average for the resulting half-lives' values is 122.303(32) s with a Birge ratio [24] of 1.1(1). This Birge ratio, relatively consistent with a value of 1, is a first indication of the absence of large systematic effects between different cycles. The red lines in Fig. 4 indicate the range defined by the uncertainty band centered on the weighted average, 122.303 $\pm$ 0.032 s.

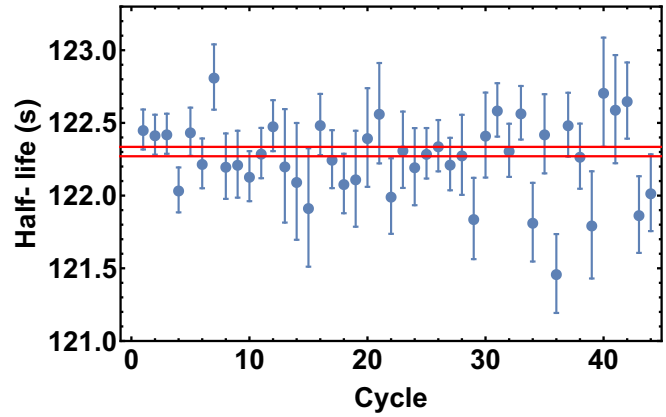

FIG. 4. The half-life resulting from fitting each individual cycle independently according to Eq. (2), along with the uncertainty band centered on the weighted average of the fitted half-lives. The larger uncertainty and spread in half-lives for latter cycles is mostly due to lower statistics.

1. Systematics check

To further probe the impact of systematic effects, the runs were investigated according to their initial activity and background as provided by the fit. These results are shown in Fig. 5. There are no trends identified in either plot, which ensures that all cycles are consistent.

B. Systematic subgroup sum fit

After determining that all runs should be included in the analysis, they were grouped by the systematic setting used. The two settings varied were photomultiplier tube (PMT) bias and threshold voltage of the discriminator. All combinations of a photomultiplier tube bias of 950, 1000, and 1050 V and a discriminator threshold of -0.3, -0.5, and -0.7 V leading to a sufficient initial activity were studied. The results are shown in Fig. 6. Also shown is the same error band from Fig. 4 as a comparison to see if any specific combination of systematic settings caused a bias in the measurement. Due to the statistically consistent nature of each combination of systematics, identified as such due to a Birge ratio of 1.2(2), it was determined that no large systematic trends were present. There is, however, by visual observation of Fig. 6, a slight trend with PMT voltage, which provided impetus for further investigation.

To address the slight trend with PMT voltage, the runs were further regrouped in three separate manners, according to PMT voltage, discriminator threshold voltage, and irradiation time. The weighted average of the results was calculated for

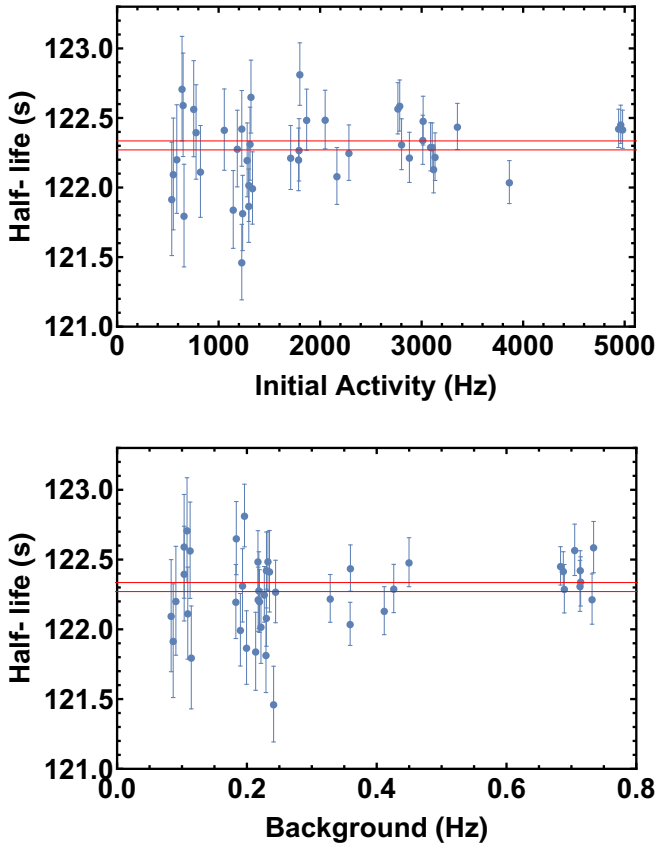

FIG. 5. The same half-life results and uncertainty band from Fig. 4 resulting from fitting cycles individually, plotted according to initial activity and background [r_0 and b from Eq. (2), respectively].

all three distinctions along with the Birge ratio to provide a measure of the data's consistency as outlined in Table II. Since the Birge ratio resulting from grouping runs according to PMT voltage gives the largest value greater than unity, a factor of 1.4 was used to scale the statistical uncertainty resulting from the total sum fit calculated in Sec. III C.

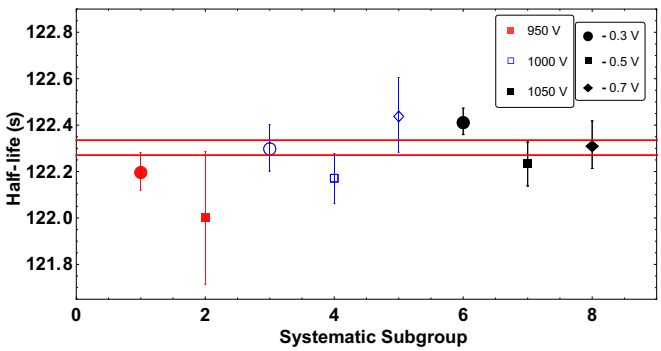

FIG. 6. Half-life resulting from summing cycles which were obtained with identical systematic settings for the photomultiplier tube voltage (color/fill) and threshold voltage (shape). Also given for comparison is the same red error band from Fig. 4.

TABLE II. Fitted half-life results along with Birge ratios when cycles are summed according to various systematic settings varied during the experiment.

Systematic setting	$t_{1/2}$ (s)	Birge ratio
PMT voltage bias	122.307(33)	1.4(3)
Discriminator threshold	122.307(33)	1.3(3)
Irradiation time	122.309(33)	0.5(3)

C. Total sum fit

After determining that all cycles were consistent, a high statistics result was determined by summing the first 3200 seconds of data from each cycle into a single decay curve shown in Fig. 7. The top panel gives the data, combined into 500 bins, as blue circles with the fit of Eq. (2) as the red line. The bottom panel gives the residuals of the fit divided by the square root of the number of counts in the given bin, shown as blue circles, along with the solid red line depicting the five-point moving average of the normalized residuals. The resulting fit gives a ^{15}O half-life of 122.308(33) s, which is in excellent agreement with the cycle-by-cycle result from Sec. III A. The statistical uncertainty resulting from this fit is then scaled according to the Birge ratio of 1.4, as described in Sec. III B, to give a more conservative result of 122.308(46).

D. Uncertainty estimation

The impacts of various sources of uncertainty were taken into consideration. These include the dead time, binning, the

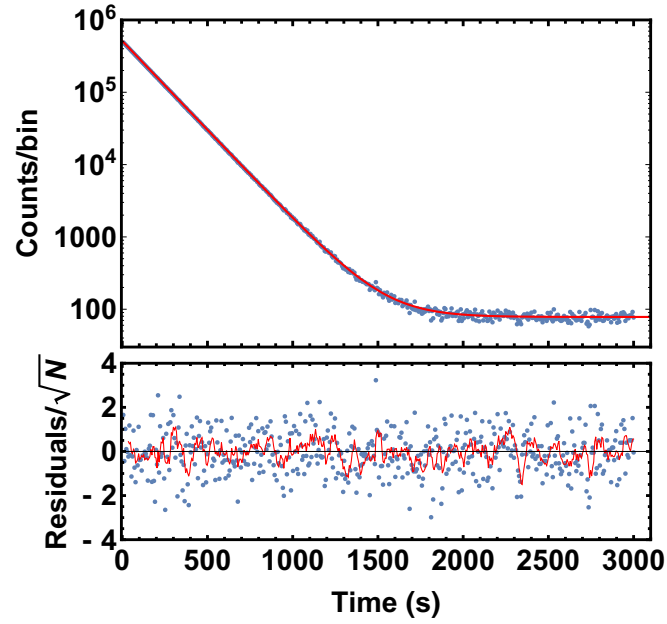

FIG. 7. The top panel gives the summed β decay curve of all cycles from this measurement of the ^{15}O half-life along with the fit according to Eq. (2). The bottom panel gives the normalized residuals from the fit along with a five-point moving average of the normalized residuals to probe for any trends in the fit.

TABLE III. Sources of systematic uncertainty on this measurement of the ^{15}O half-life.

Source	Uncertainty (ms)
Dead time	15
Binning	0.70
Cycle grouping	4.7
Clock time	0.13
Fitting routine	9×10^{-3}
Total systematic uncertainty	16

cycle summing method, the clock time, and the fit routine. The potential of a measurement bias resulting from beam contamination was also further investigated. The resulting systematic uncertainty of the half-life was 16 ms as outlined in Table III, with the total systematic uncertainty calculated resulting from the sum of all individual contributions added in quadrature. This inflates the total uncertainty in the measurement from 46 ms to 49 ms. Details for the determination of each source of systematic uncertainty are given in the following sections.

1. Dead time

The online dead time was determined by taking the difference between two clock time measurements of each cycle time. One clock was always running to record the total time of each cycle, while the other clock was vetoed, along with the rest of the data acquisition, for a set period of time after each trigger while counts were being processed. This ensured we had a nonparalyzing dead time. The difference between the two clock times divided by the total number of counts per cycle gave the dead time for each individual cycle. The result, 55.94 μs, was the average of the dead times from each cycle, and the uncertainty was given by the standard deviation of the data set divided by the square root of the total number of cycles, 0.25 μs. To obtain a more precise dead-time value, after the experiment concluded the system ran with a radioactive source and pulser for an extended period of time to gain better statistics. This resulted in an offline dead-time measurement of 56.32(16) μs. The overall dead time was then conservatively calculated by taking the weighted average of the online and offline results and inflating the error on the weighted average by the Birge ratio of 1.3(3). The resulting dead time was determined to be 56.22(18) μs. The impact of this uncertainty on the final value of the half-life was determined by performing sum fits at both extremes of the dead time, 56.04 and 56.40 μs. The uncertainty was taken as half the difference between the two resulting fits, 15 ms. This influence dominates the systematic uncertainty for this experiment, as it is a factor of 3 larger than any other contribution.

2. Binning

The number of time bins for each fit was chosen to be 500 to minimize the number of empty bins; however, the effect of choosing more or fewer bins was also considered. As a systematic check, fits were also done with 250 and 1000 bins. The systematic uncertainty contribution was calculated as half of the largest difference between the resulting half-life values, 0.70 ms.

3. Cycle grouping

The influence of adding all the cycles together for the sum fit was probed by determining the half-life for various groupings of cycles, as described in Secs. III A, and III B. When cycles were fit individually, the weighted average of the results was 122.303(35) s compared to 122.306(39) s when the systematic subgroups were summed together. The biggest discrepancy with the sum of all cycles was from the individual cycle fitting, so the difference, 4.7 ms, was taken as an additional systematic uncertainty.

4. Clock time

The frequency of the clock pulse was measured to be 99.9996(10) Hz using a Teledyne Lecroy 500 MHz oscilloscope. As done with the dead time, sum fits were repeated with extreme clock times at both of the extremes of frequency set by the uncertainty, and then half the difference was taken as an additional systematic uncertainty. This resulted in a small contribution to the overall systematic uncertainty, at 0.13 ms.

5. Fit routine

The analysis followed the method prescribed by [23] to determine the half-life, as successfully done in previous measurements with the β-Counting Station. To determine if this introduced a strong bias on the result, a second fitting routine which minimized a χ^2 determined by Poisson statistics was used as a comparison [25]. This method converged on fit parameters with a reduced χ^2_ν of 0.96 for the data from Fig. 7. Half the difference between this fitting method and the result from the sum fit, 8.6×10^{-3} ms, was added to the overall systematic uncertainty; however an influence of this order has no impact relative to other more dominant sources.

6. Beam contamination

Although the particle identification plot in Fig. 2 indicates the absence of radioactive contamination, the potential influence of a small unidentified contaminant was still considered in the analysis to ensure there was nothing below the threshold of online investigations which could still bias the measured half-life at the reported precision. The first test was to fit the sum of all data with a decay rate which included an added contribution of a contaminant with half-life t_2 given as

$$r(t) = r_0\{\exp[-\ln(2)t/t_1] + \alpha \exp[-\ln(2)t/t_2]\} + b, \quad (3)$$

where α is the ratio of the initial activity for the contaminant divided by the initial activity of ^{15}O, and t_1 is the half-life of ^{15}O. The data were then fit following the same fitting routine used previously with the updated decay rate equation. Various values were used as the initial guess for the t_2 fit parameter including 0.01, 0.1, 1, 60, 100, 200, 250, 500, and 1000 s. All contaminant half-life values provided for the routine determined values of α consistent with zero, signifying the absence of contamination.

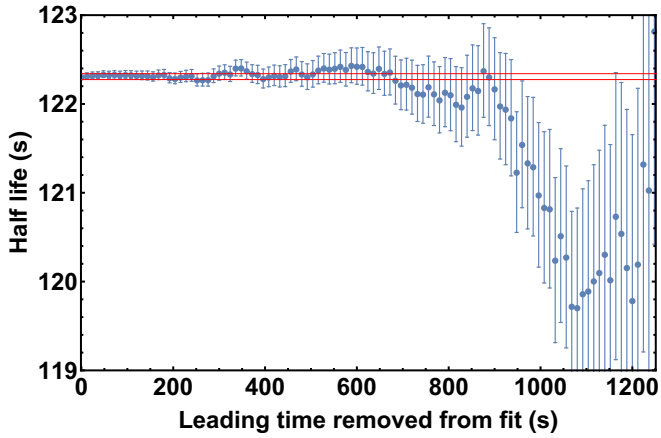

FIG. 8. Chop plot for the sum of all cycles, where each point is the half-life resulting from fitting the data after progressively removing bins from the beginning of all cycles. Systematic trends would present themselves here by a trend beyond statistical fluctuation about the mean shown as the region bound by the solid red lines.

Furthermore, potential short-lived contaminants along with a possible incorrect evaluation of the dead time were probed by removing the leading bins, one at a time, and then redetermining the half-life with the remaining data following a procedure identical to the sum fit from Sec. III C. The results from these fits, where up to ten half lives were removed, shown in Fig. 8 and referred to as a chop plot, show consistent results lacking any time dependent effects outside normal statistical fluctuation about the initial value up to the point where fitting ^{15}O breaks down due to its near absence on the foil after decaying away. This further solidified the conclusion that there was no contamination which influenced this measurement of the half-life.

The final search for contamination occurred by looking for long-lived contamination by repeating the sum fitting procedure from Sec. III C for the eight long cycles that were taken periodically throughout the measurement period. The results are shown in Fig. 9. The five-point moving average in the lower panel clearly randomly oscillates about the constant background value for the entire range (about 6000 s) after all ^{15}O has decayed away, which is a clear indication of the lack of a long-lived contaminant's presence on the paddle. To further probe the presence of relatively long-lived contamination, which could be identified as a nonzero slope on the background, the eight long cycles were additionally fit with the function

$$r(t) = r_0\{\exp[-\ln(2)t/t_1]\} + mt + b, \tag{4}$$

where m is the slope of the background. The long runs give increased statistics to fit this additional term, and the results again indicate the absence of contamination with a value of m consistent with zero as $(0.6 \pm 2.6) \times 10^{-6}$.

The combination of all these considerations led to the conclusion that there were no other radioactive species present which affected this half-life measurement at the reported precision.

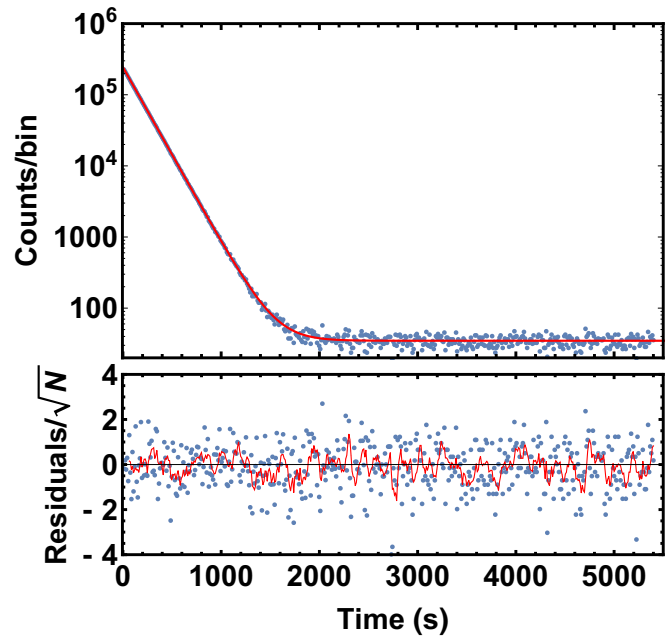

FIG. 9. Identical to Fig. 7 for the eight long cycles to probe long-lived contamination.

IV. ^{15}O HALF-LIFE

As outlined in previous sections, this work reports a new half-life measurement of ^{15}O of $t_{1/2} = 122.308(49)$ s. This is in agreement with the previous world average but significantly more precise than any previous measurement. Utilizing this half-life measurement, a new world average is calculated by considering all previous measurements with uncertainties better than ten times the uncertainty of the most precise measurement. The world average is then calculated to be 122.266(43) s, with all results outlined in Fig. 10. The Birge ratio of these three measurements is 1.3, which is an improvement over the

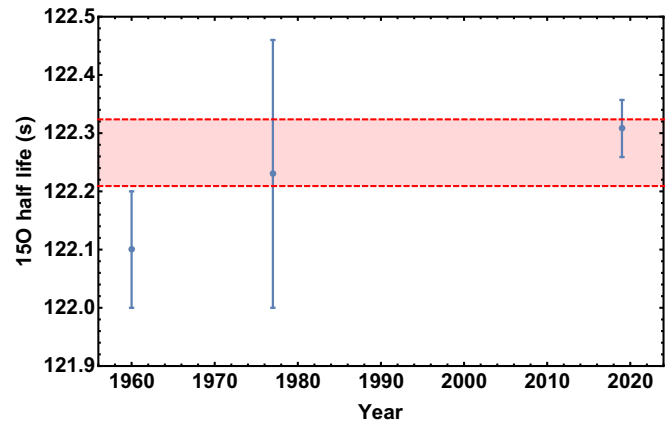

FIG. 10. Summary of the measurements included in the updated world average. Only previous measurements with a precision better than ten times the measurement outlined in this paper are included in this consideration, aligning with practices of the Particle Data Group. The red (shaded) region gives the world average with the error enlarged by the Birge ratio of 1.3

TABLE IV. Outline of the parameters used in this evaluation of $\mathcal{F}t^{\text{mirror}}$ using ^{15}O.

Parameter	Value	Reference
$t_{1/2}$	122.27(6) s	This work
f_v	35.502(43)	This work, [26,27]
BR	100%	[6]
P_{EC}	0.1%	[6]
δ_R'	1.555(8)%	[6]
$\delta_{NS}^V - \delta_C^V$	0.22(3)%	[6]
$\mathcal{F}t^{\text{mirror}}$	4422.8(59) s	

previous compilation's value of 2.6 and therefore indicates that a more consistent data set has been used in this evaluation of the world average. With consideration of this Birge ratio, the uncertainty of the new world average is scaled accordingly to give $t_{1/2}^{\text{world}} = 122.27(6)$ s.

V. DISCUSSION

With this measurement of the ^{15}O half-life, the uncertainty of the world average has decreased by a factor of 4, which has implications for the calculation of $\mathcal{F}t^{\text{mirror}}$ defined in Eq. (1). The values used to calculate $\mathcal{F}t^{\text{mirror}}$ are outlined in Table IV, with the updated result being 4422.8(59) s. Figure 11 gives the fractional uncertainty of each value required in this calculation of $\mathcal{F}t^{\text{mirror}}$ to show that the half-life was previously the dominating quantity but now is on par with the theoretical corrections. This further incentivizes a more precise determination of the Q_{EC} value to bring all uncertainties down to the same order of magnitude.

It should be noted that $\mathcal{F}t^{\text{mirror}}$ is the analog of $\mathcal{F}t^{\,0^+\to0^+}$ applied to mirror decays which, unlike the pure Fermi cases, is not equivalent for all mirror decays due to the nonzero Gamow-Teller term of the nuclear transition matrix element. Therefore, the inclusion of an axial-vector term in the calculation of the more general $\mathcal{F}t_0^{\text{mirror}}$ is of interest when testing the standard model, as it is equivalent for all mixed mirror decays. For $T = 1/2$ mixed mirror decays, $\mathcal{F}t_0^{\text{mirror}}$ can be defined in terms of the Fermi to Gamow-Teller mixing ratio, ρ, as

$$\mathcal{F}t_0^{\text{mirror}} = f_v t(1+\delta_R')(1+\delta_{NS}^V - \delta_C^V)\left(1 + \frac{f_A}{f_v}\rho\right). \quad (5)$$

However, an explicit value of ρ has never been reported for ^{15}O, and therefore one cannot extract $\mathcal{F}t_0^{\text{mirror}}$ solely from experimental quantities from this nucleus. A β-anisotropy measurement of ^{15}O was performed previously [28], and a β-anisotropy parameter (and hence a value for ρ[7]) with a relative uncertainty of 2% could be extracted if the magnetic moment μ and the hyperfine field B are known to sufficient accuracy [28]. Therefore, we must rather rely on the absolute validity of the standard model and proceed by predicting the expected value of ρ using $\mathcal{F}t^{\,0^+\to0^+} = 3072.27(72)$ s [2] according to

$$\rho^2 = \frac{f_v}{f_A}\left(2\,\frac{\mathcal{F}t^{\,0^+\to0^+}}{\mathcal{F}t^{\text{ mirror}}} - 1\right). \quad (6)$$

This determination gives $\rho = -0.623(2)$ for ^{15}O. Solutions of ρ in Eq. (6) provide two possibilities for the sign; however, the absolute sign can be determined by shell model calculations [6]. An explicit measurement of this value is of great interest to test the completeness of the standard model.

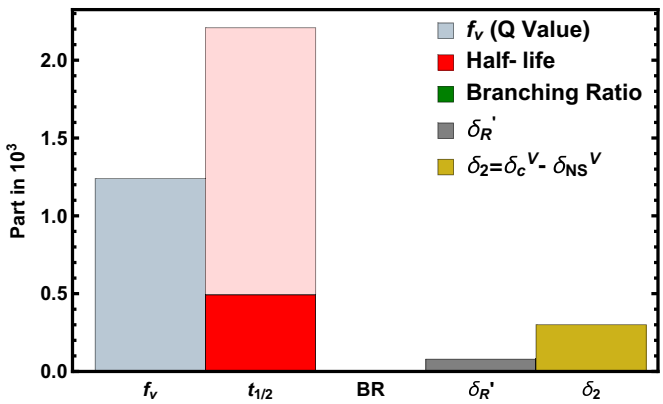

FIG. 11. Fractional uncertainties for all quantities required in this calculation of $\mathcal{F}t^{\text{mirror}}$ using ^{15}O. Shown in light red is the previous contribution from the half-life before this measurement, while the dark red gives the updated value which is now on par with the theoretical corrections.

VI. OUTLOOK

We have conducted the most precise half-life measurement to date for ^{15}O with a factor of 2 better precision than any previous measurement. This resulted in a greatly reduced uncertainty in the world average of 122.27(6) s compared to the previous compilation's result of 122.24(23) s. The dominant source of uncertainty in the calculation of $\mathcal{F}t^{\text{mirror}}$ is now the statistical rate function, which can be reduced with a more precise measurement of the Q_{EC} value. An improvement of this quantity to the level of precision of the reported half-life will be important, in anticipation for a future explicit measurement of the Fermi to Gamow-Teller mixing ratio of ^{15}O. Such a measurement is on the horizon with the St. Benedict ion trapping system [8,9].

ACKNOWLEDGMENT

This work was supported in part by the National Science Foundation (NSF) under Grants No. PHY-1713857, No. PHY-1401242, and No. PHY-1401343.

[1] J. C. Hardy and I. S. Towner, J. Phys. G: Nucl. Part. Phys. **41**, 114004 (2014).
[2] J. C. Hardy and I. S. Towner, Phys. Rev. C **91**, 025501 (2015).
[3] C.-Y. Seng, M. Gorchtein, H. H. Patel, and M. J. Ramsey-Musolf, Phys. Rev. Lett. **121**, 241804 (2018).
[4] A. Czarnecki, W. J. Marciano, and A. Sirlin, Phys. Rev. D **100**, 073008 (2019).
[5] W. Satuła, J. Dobaczewski, W. Nazarewicz, and T. R. Werner, Phys. Rev. C **86**, 054316 (2012).
[6] N. Severijns, M. Tandecki, T. Phalet, and I. S. Towner, Phys. Rev. C **78**, 055501 (2008).
[7] O. Naviliat-Cuncic and N. Severijns, Phys. Rev. Lett. **102**, 142302 (2009).
[8] D. Burdette, M. Brodeur, P. O'Malley, and A. Valverde, Hyperfine Interact. **240**, 70 (2019).
[9] A. A. Valverde, M. Brodeur, D. P. Burdette, J. A. Clark, J. W. Klimes, D. Lascar, P. D. O'Malley, R. Ringle, G. Savard, and V. Varentsov, Hyperfine Interact. **240**, 38 (2019).
[10] B. Fenker, A. Gorelov, D. Melconian, J. A. Behr, M. Anholm, D. Ashery, R. S. Behling, I. Cohen, I. Craiciu, G. Gwinner *et al.*, Phys. Rev. Lett. **120**, 062502 (2018).
[11] M. Gonzalez-Alonso, O. Naviliat-Cuncic, and N. Severijns, Prog. Part. Nucl. Phys. **104**, 165 (2019).
[12] B. Ohayon, H. Rahangdale, E. Parnes, G. Perelman, O. Heber, and G. Ron, Phys. Rev. C **101**, 035501 (2020).
[13] M. Brodeur, C. Nicoloff, T. Ahn, J. Allen, D. W. Bardayan, F. D. Becchetti, Y. K. Gupta, M. R. Hall, O. Hall, J. Hu *et al.*, Phys. Rev. C **93**, 025503 (2016).
[14] J. R. Penning and F. H. Schmidt, Phys. Rev. **105**, 647 (1957).
[15] O. C. Kistner and B. M. Rustad, Phys. Rev. **114**, 1329 (1959).
[16] J. Janecke, Z. Naturforsch. A **15**, 593 (1960).
[17] J. W. Nelson, E. B. Carter, G. E. Mitchell, and R. H. Davis, Phys. Rev. **129**, 1723 (1963).
[18] G. Azuelos, J. E. Kitching, and K. Ramavataram, Phys. Rev. C **15**, 1847 (1977).
[19] F. D. Becchetti, M. Y. Lee, T. W. O'Donnell, D. A. Roberts, J. J. Kolata, L. O. Lamm, G. Rogachev, V. Guimarães, P. A. DeYoung, and S. Vincent, in Proceedings of the Tenth Symposium on Radiation Measurements and Applications [Nucl. Instrum. Methods Phys. Res., Sect. A **505**, 377 (2003)].
[20] J. Long, T. Ahn, J. Allen, D. W. Bardayan, F. D. Becchetti, D. Blankstein, M. Brodeur, D. Burdette, B. Frentz, M. R. Hall *et al.*, Phys. Rev. C **96**, 015502 (2017).
[21] A. A. Valverde, M. Brodeur, T. Ahn, J. Allen, D. W. Bardayan, F. D. Becchetti, D. Blankstein, G. Brown, D. P. Burdette, B. Frentz *et al.*, Phys. Rev. C **97**, 035503 (2018).
[22] D. P. Burdette, M. Brodeur, T. Ahn, J. Allen, D. W. Bardayan, F. D. Becchetti, D. Blankstein, G. Brown, B. Frentz, M. R. Hall *et al.*, Phys. Rev. C **99**, 015501 (2019).
[23] V. Koslowsky, E. Hagberg, J. Hardy, G. Savard, H. Schmeing, K. Sharma, and X. Sun, Nucl. Instrum. Methods Phys. Res., Sect. A **401**, 289 (1997).
[24] R. T. Birge, Phys. Rev. **40**, 207 (1932).
[25] G. F. Grinyer, C. E. Svensson, C. Andreoiu, A. N. Andreyev, R. A. E. Austin, G. C. Ball, R. S. Chakrawarthy, P. Finlay, P. E. Garrett, G. Hackman *et al.*, Phys. Rev. C **71**, 044309 (2005).
[26] W. Huang, G. Audi, M. Wang, F. G. Kondev, S. Naimi, and X. Xu, Chin. Phys. C **41**, 030002 (2017).
[27] I. S. Towner and J. C. Hardy, Phys. Rev. C **91**, 015501 (2015).
[28] N. Severijns, J. Wouters, J. Vanhaverbeke, and L. Vanneste, Phys. Rev. Lett. **63**, 1050 (1989).